JACS
JOURNAL OF THE AMERICAN CHEMICAL SOCIETY
Communication
pubs.acs.org/JACS

Dynamic Characterization of Crystalline Supramolecular Rotors Assembled through Halogen Bonding

Luca Catalano,[†,‡] Salvador Pérez-Estrada,[‡] Giancarlo Terraneo,*[,†] Tullio Pilati,[†] Giuseppe Resnati,[†] Pierangelo Metrangolo,*[,†,§] and Miguel A. Garcia-Garibay*[,‡]

[†]Laboratory of Nanostructured Fluorinated Materials (NFMLab), Department of Chemistry, Materials, and Chemical Engineering "Giulio Natta", Politecnico di Milano, via L. Mancinelli 7, 20131 Milano, Italy

[‡]Department of Chemistry and Biochemistry, University of California, Los Angeles, California 90095-1569, United States

[§]VTT-Technical Research Centre of Finland, P.O. Box 1000, Espoo FI-02044, Finland

Supporting Information

ABSTRACT: A modular molecular kit for the preparation of crystalline molecular rotors was devised from a set of stators and rotators to gain simple access to a large number of structures with different dynamic performance and physical properties. In this work, we have accomplished this with crystalline molecular rotors self-assembled by halogen bonding of diazabicyclo[2.2.2]octane, acting as a rotator, and a set of five fluorine-substituted iodobenzenes that take the role of the stator. Using variable-temperature ^{1}H T_1 spin−lattice relaxation measurements, we have shown that all structures display ultrafast Brownian rotation with activation energies of 2.4−4.9 kcal/mol and pre-exponential factors of the order of (1−9) × 10^{12} s^{-1}. Line shape analysis of quadrupolar echo ^{2}H NMR measurements in selected examples indicated rotational trajectories consistent with the 3-fold or 6-fold symmetric potential of the rotator.

Amphidynamic crystals are materials specifically designed to possess rapidly moving components (rotators) in the solid state.[1] It is expected that these materials may provide a suitable platform for the development of future functional materials and artificial molecular machines.[1,2] Typically, molecular design in this field has taken inspiration from structures akin to those of macroscopic compasses and gyroscopes to explore and control rotation in the solid state.[3] Rotation in solids has been studied in molecular crystals,[3] inclusion compounds,[4] metal−organic frameworks,[5] porous molecularly ordered silicates,[6] and amorphous solids.[7]

Here we take advantage of the principles of crystal engineering[8] to assemble stators and rotators into co-crystals, which results in the high-yield synthesis of active supramolecular rotor arrays. Advantages of this strategy originate from the intrinsic flexibility and its modular design, thanks to the wide variety of supramolecular synthons[8] available in the crystal engineering toolbox. Furthermore, the dynamic performance of the supramolecular rotor may be tuned by controlling the non-covalent interactions involving stators and rotators in the crystal structures.

Among the wide variety of non-covalent interactions available, such as metal coordination, Coulombic interactions, hydrogen bonding (HB), and $\pi-\pi$ stacking, halogen bonding (XB) has only been used once for the design of amphidynamic crystals.[9,10] In particular, it was demonstrated recently that bis(1,4-iodoethynyl)bicyclo[2.2.2]octane showed ultrafast rotation when self-assembled in crystalline XB networks through iodine−acetylene interactions at the two ends of each rotator.[11] Under the hypothesis that the halogen bond, thanks to its strength, directionality, selectivity, and tunability, may provide an extra value in the design of co-crystals showing dynamic components, we studied molecular motions of a series of XB co-crystals involving 1,4-diazabicyclo[2.2.2]octane (DABCO),[12] a well-known C_3-symmetric and cylindrically shaped rotator that packs in a manner that does not generate high rotational barriers.[11,13]

The commercially available fluoro-substituted iodobenzenes (F_nPheI) **1a−e** were chosen as powerful XB donors that can play the role of stators when assembled with the DABCO rotator via F_nPheI···NR_3 interactions (Figure 1). We anticipated that compounds **1a−e** would simultaneously offer a suitable static platform, a non-covalent axle, the halogen bond, and a frame of reference for the rotation of DABCO.

Self-assembly experiments were carried out by mixing in acetone solutions 2 equiv of **1a−e** per equivalent of DABCO,

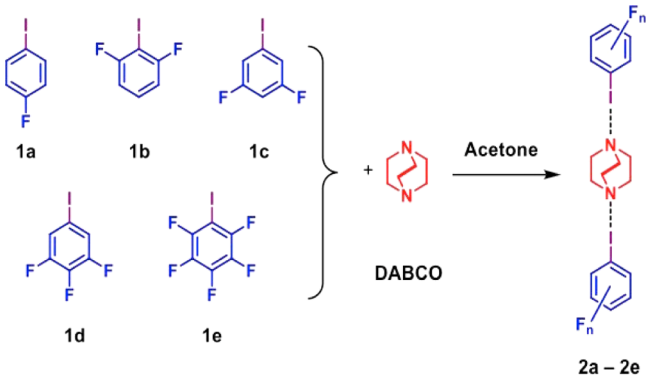

Figure 1. Self-assembly of the fluoro-substituted iodobenzenes (F_nPheI) **1a−e** and DABCO, resulting in crystalline halogen-bonded molecular rotors **2a−e**.

Received: October 14, 2015
Published: November 19, 2015

DOI: 10.1021/jacs.5b10776
J. Am. Chem. Soc. 2015, 137, 15386−15389

taking into account the mono- and bidentate nature of **1a–e** and DABCO, respectively, as far as the XB donor/acceptor sites are concerned. Upon slow solvent evaporation, crystalline solids were obtained in all cases with melting points different from those of the starting compounds and ranging from 311 to 378 K (Table 1). Peak integration of the ^{1}H NMR spectra

Table 1. Melting Points, Space Groups, and Arrhenius Parameters for Rotational Dynamics from the Kubo–Tomita Fit of the T_1 Data for DABCO and the Related Halogen-Bonded Co-crystals 2a–e

compd/co-crystal (mp, K)	space group (Z)	E_a (kcal/mol)[a]	τ_0^{-1} (s^{-1})	C ($\times 10^8$ s^{-2})
DABCO (429)	$P6_3/m$[b] (2)	8.2[c]	1.3×10^{14}[c]	n.a.
2a (318–321)	$C2/c$ (4)	4.8	9.9×10^{12}	5.2
2b (334–336)	$P2_1/n$ (4)	2.7	2.0×10^{12}	7.4
2c (344–345)	$P2_1/c$ (4)	2.4	1.1×10^{12}	6.5
2d (311–314)	$P2_1/c$ (2)	2.8	2.3×10^{12}	5.0
2e (377–378)	$P2_1/c$ (2)	3.6	2.3×10^{12}	7.5

[a]Data obtained at 297 K; Z is the number of molecules per asymmetric unit. [b]Reference 14a. [c]Reference 14b.

confirmed that all of the complexes except **2c** showed the expected 2:1 ratios of the starting compounds; **2c**, instead, showed a 1:1 ratio between **1c** and DABCO.

Good-quality single crystals of the obtained co-crystals **2a–e** were submitted to X-ray diffraction (XRD) analysis, which was in all cases carried out at 103 K. Structural analysis confirmed the starting design of the desired XB motif with both the N-atoms of DABCO working as XB acceptors toward the I-atoms of two different F_nPheI modules, resulting in trimeric complexes. In contrast, the structure of complex **2c** consisted of 1D infinite chains in which **1c** and DABCO alternated as a consequence of the ditopic nature of **1c**, which also behaved as a HB donor through the H-atom in the *para*-position to the I-atom in the benzene ring (Figure 2b). This explains the 1:1 ratio observed for this complex through ^{1}H NMR analysis, regardless of starting from either a 1:1 or 2:1 mixing ratio.

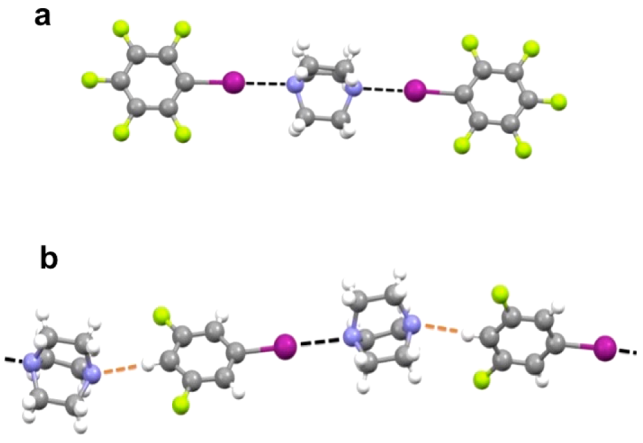

Figure 2. (a) Halogen-bonded trimer in the crystal structure of **2e**. (b) 1D infinite chain in **2c** due to the simultaneous XB and HB donor behavior of **1c** when mixed with DABCO. HB geometrical parameters are C···N = 3.348(3) Å and C–H···N = 174.0(1)°. Color code: C, gray; H, white; N, sky blue; F, light green; I, magenta. XB and HB are represented as black and orange dashed lines, respectively.

The halogen bonds observed in complexes **2a–e** are characterized by short I···N distances (2.79 Å on average) and almost linear C–I···N angles (176.7° on average), as shown in Table 2. The XB becomes shorter, and thus stronger, with

Table 2. Halogen Bonds and Angles in 2a–e at 103 K

complex	N···I (Å)	N···I—C (deg)
2a	2.971(4), 2.955(4)[a]	176.32(2), 175.51(2)[a]
2b	2.857(2), 2.732(2)[a]	173.86(8), 179.12(8)[a]
2c	2.832(1)	175.19(4)
2d	2.815(6)	175.8(2)
2e	2.713(1), 2.682(1), 2.681(1), 2.701(1)[a]	177.04(5), 178.64(5), 177.96(5), 177.19(5)[a]

[a]Independent halogen bonds.

the increase of the fluorination degree of the stator, and hence the magnitude of the iodine σ-hole.[16] Similarly, *m*-fluorination may explain why **1c** behaves as a HB donor, while **1b** does not. No other driving non-covalent interactions characterize the crystal packing of these complexes.[15] Importantly, NMR, IR, thermal, and powder XRD analyses confirmed the above-described co-crystals were obtained in quantitative bulk.

To explore structural changes and the dynamics of DABCO in the complexes **2a–e** when the temperature was changed, we performed variable-temperature (VT) single-crystal XRD, ^{1}H T_1 NMR, and wide-line quadrupolar echo ^{2}H NMR analyses. It is known that changes in the size and orientation of the anisotropic thermal parameters may be related to the potential energy that determines dynamic processes in crystals.[16] On heating single crystals of the complexes **2a** and **2e** from ∼100 K to room temperature, reversible phase transitions without substantial modifications of the crystal packing were recorded. These occurred at ∼280 and 230 K, respectively, as shown in detail in the Supporting Information (SI). For **2e**, XRD data were collected in the range 103–298 K, following five intermediate steps (140, 180, 200, 220, and 250 K). On increasing the temperature of the XRD acquisition, increasing rotational disorder of the DABCO $-CH_2CH_2-$ alkyl bridges was observed, which has to be expected from a thermally activated rotational process (Figure 3). Conversely, the

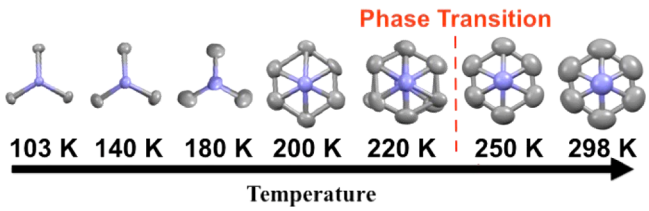

Figure 3. Views along the N–N axis of the DABCO component in co-crystal **2e**, which show increasing disorder of the alkyl bridges, in terms of larger thermal ellipsoids and splitting over two positions as a function of temperature from 103 to 298 K.

pentafluoroiodobenzene module only showed disorder in the plane of the aromatic ring (see SI). Similar motion and disorder were also observed for the co-crystals **2a–d**.

Spin–lattice relaxation measurements have been used to document dynamic processes in the vicinity of the Larmor frequency[18] (300 MHz for ^{1}H T_1 measurements in this case). This method is well suited for crystalline solids, in which the main mechanism of relaxation is due to the motion-mediated fluctuation of magnetic fields arising from dipolar coupling

DOI: 10.1021/jacs.5b10776
J. Am. Chem. Soc. 2015, 137, 15386–15389

among H-atoms. In the case of the co-crystals **2a**–**e**, the rotation of DABCO is the predominant thermally activated process, with dynamics characterized by a correlation time (τ_c), which follows an Arrhenius-type behavior (eq 1). Under these conditions, it is possible to obtain its activation energy (E_a) and pre-exponential factor (τ_0^{-1}) by fitting the measured T_1 data as a function of temperature to the Kubo–Tomita (KT) relaxation expression (eq 2), by substituting the τ_c term with eq 1.

$$\tau_c^{-1} = \tau_0^{-1} \exp(-E_a/RT) \quad (1)$$

$$T_1^{-1} = C[\tau_c(1 + \omega_0^2\tau_c^2)^{-1} + 4\tau_c(1 + 4\omega_0^2\tau_c^2)^{-1}] \quad (2)$$

The parameter C in eq 2 is a constant related to the strength of the homonuclear dipolar interactions, which, as expected, are similar for all of the studied co-crystals (see Table 1), and ω_0 is the Larmor frequency (for further details, please refer to the SI). Good KT fitting of the experimental data were obtained, allowing the determination of the Arrhenius parameters reported in Table 1.

As illustrated in Figure 4, with a $\ln(T_1^{-1})$ vs $1000/T$ (K) plot of the experimental data obtained on co-crystal **2e**, there is a

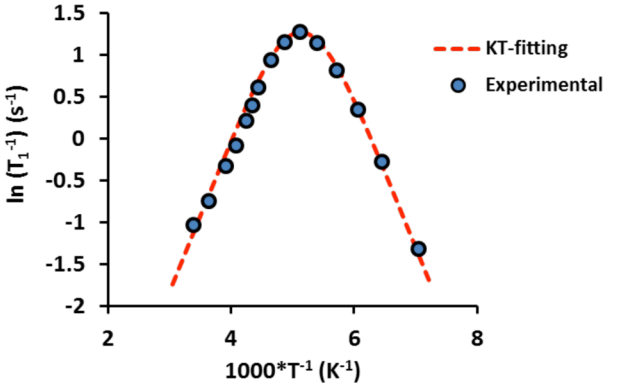

Figure 4. ^{1}H spin–lattice relaxation times (^{1}H T_1) measured for **2e** on cooling from 295 to 141 K at 300 MHz (solid blue circles). The plot $\ln(T_1^{-1})$ vs $1000T^{-1}$ shows a maximum at ~195 K. The red dotted line corresponds to the Kubo–Tomita fit of the experimental data.

single maximum at ~195 K, with an excellent KT fit for a single dynamic process with an exceptionally low $E_a \approx 3.6$ kcal/mol and $\tau_0^{-1} = 2.3 \times 10^{12}$ s^{-1}. Similar behaviors were obtained also for **2a**–**d**, with $E_a = 2.4$–4.9 kcal/mol (Table 1). Notably, data obtained from co-crystal **2a** showed a discontinuity that correlates with a phase transition that occurs in the range 285–310 K (Figure S17). While it was not possible to fit the experimental data in the high-temperature phase due to the small number of experimental points in the proximity of the crystal melting, the dynamics of the low-temperature phase was fully characterized, with $E_a = 4.9$ kcal/mol and $\tau_0^{-1} = 9.9 \times 10^{12}$ s^{-1}.

The activation energies measured for co-crystals **2a**–**e** are considerably lower than the activation energy for rotation reported in the case of pure crystalline DABCO, which has $E_a = 8.2$ kcal/mol and $\tau_0^{-1} = 1.3 \times 10^{14}$ s^{-1} (Table 1). This may probably be due to the fact that rotator molecules in the reported XB co-crystals are partially isolated from neighboring rotators by the XB donors **1a**–**e**, which thus function as bearings and stators (Figure 5).

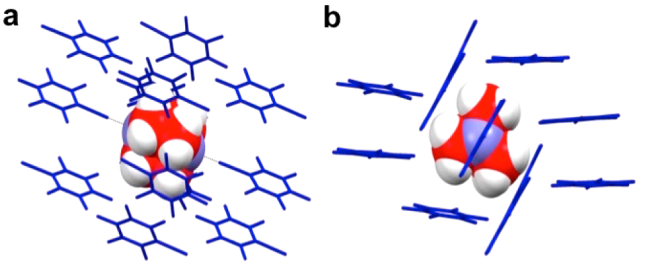

Figure 5. Views along the *b* crystallographic axis (a) and along the N–N molecular axis (b) of the crystal structure of **2e**, showing the isolation of a DABCO rotator (red) by neighboring pentafluoroiodobenzene modules in blue.

The higher activation energy for rotation of pure DABCO may be associated with the closer rotator–rotator distances and steric interactions in the crystal. The pre-exponential factor is related to the frequency of oscillations within the local energy well and can be associated with an attempt frequency for rotational jumps that is determined by both thermal energy and the size of the activation barrier ($-E_a/RT$). The attempt frequency corresponds to the rotational exchange frequency that would occur in the absence of a barrier, i.e., when $E_a = 0$. Notably, the τ_0^{-1} values obtained for the XB co-crystals **2a**–**e** are comparable to those determined for other amphidynamic crystals with analogous DABCO-based molecular rotators linked to the stators by covalent bonds.[11,13] This suggests that the XB molecular rotors reported in this Communication may be as efficient as similar rotors based fully on covalent bonds. However, in co-crystal **2c**, it was not possible to discern the different contributions of XB and HB to the rotational dynamics of the supramolecular rotor.

To elucidate the trajectories of motion, three supramolecular rotors, **2a**, **2b**,and **2e**, were taken as models and their dynamics studied by wide-line quadrupolar echo ^{2}H NMR.[18] The sample co-crystals were prepared by using perdeuterated DABCO obtained by H/D exchange reaction using Raney nickel and D_2O.[19] For the three studied systems, the wide-line spectra collected between 140 and 295 K did not show any appreciable changes, in good agreement with the high rotational frequencies expected from the low E_a and high τ_0^{-1} values. The simulated spectra[20] suggested a dynamical process in which DABCO rotates around its N–N axis in the fast-exchange regime. The experimental data coupled with the simulations are consistent with either a 3-site or 6-site potential of the rotator; see example in Figure 6.

In conclusion, a series of two-component amphidynamic co-crystals with very efficient rotational dynamics were readily prepared from simple and commercially available building blocks by taking advantage of a crystal engineering strategy based on the use of XB. The reported systems are the first examples of this new class of materials. Rotational dynamics based on VT ^{1}H T_1 NMR spin–lattice relaxation revealed pre-exponential factors comparable to those found in rotors with covalent rotational axles, suggesting that the XB, and the HB in the specific case of **2c**, constitute new robust axles for molecular rotation and a new design principle in the field of molecular rotors. The discovery of these new crystalline multicomponent systems thus opens up new avenues in the development of new smart materials and molecular machines.

DOI: 10.1021/jacs.5b10776
J. Am. Chem. Soc. 2015, 137, 15386–15389

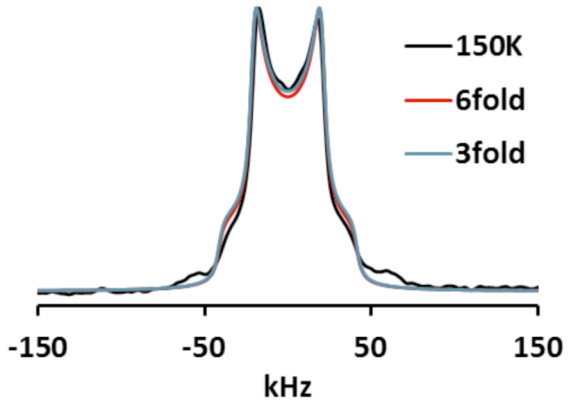

Figure 6. Deuterium wide-line spectrum of **2a** collected at 150 K (black line) compared with 3-fold and 6-fold potential simulated spectra (blue and red lines).

■ ASSOCIATED CONTENT

Supporting Information

The Supporting Information is available free of charge on the ACS Publications website at DOI: 10.1021/jacs.5b10776.

Experimental procedures, further characterization, and spectra (PDF)
X-ray data for **2e** at 220 K (CIF)
X-ray data for **2e** at 250 K (CIF)
X-ray data for **2e** at rt (CIF)
X-ray data for **2e** at 103 K (CIF)
X-ray data for **2e** at 140 K (CIF)
X-ray data for **2e** at 180 K (CIF)
X-ray data for **2e** at 200 K (CIF)
X-ray data for **2a** at 103 K (CIF)
X-ray data for **2a** at 297 K (CIF)
X-ray data for **2b** at 103 K (CIF)
X-ray data for **2b** at 253 K (CIF)
X-ray data for **2b** at rt (CIF)
X-ray data for **2c** at 103 K (CIF)
X-ray data for **2c** at 233 K (CIF)
X-ray data for **2c** at rt (CIF)
X-ray data for **2d** at 100 K (CIF)
X-ray data for **2d** at rt (CIF)

■ AUTHOR INFORMATION

Corresponding Authors

*giancarlo.terraneo@polimi.it
*pierangelo.metrangolo@polimi.it
*mgg@chem.ucla.edu

Notes

The authors declare no competing financial interest.

■ ACKNOWLEDGMENTS

M.A.G.-G. acknowledges support from the National Science Foundation (grant DMR1402682). P.M. and G.T. acknowledge support from the MIUR, PRIN 2010-2011 (grant 2010CX2TLM "InfoChem").

■ REFERENCES

(1) Vogelsberg, C. S.; Garcia-Garibay, M. *Chem. Soc. Rev.* **2012**, *41*, 1892−1910.
(2) (a) Akutagawa, T.; Shitagami, K.; Nishihara, S.; Takeda, S.; Hasegawa, T.; Nakamura, T.; Hosokoshi, Y.; Inoue, K.; Ikeuchi, S.; Miyazaki, Y.; Saito, K. *J. Am. Chem. Soc.* **2005**, *127*, 4397−4402. (b) Kottas, G. S.; Clarke, L. I.; Horinek, D.; Michl, J. *Chem. Rev.* **2005**, *105*, 1281−1376. (c) Akutagawa, T.; Koshinaka, H.; Sato, D.; Takeda, S.; Noro, S.-I.; Takahashi, H.; Kumai, R.; Tokura, Y.; Nakamura, T. *Nat. Mater.* **2009**, *8*, 342−347. (d) Hou, X.; Ke, C.; Bruns, C. J.; Mc Gonigal, P. R.; Pettman, R. B.; Stoddart, J. F. *Nat. Commun.* **2015**, *6*, 6884. (e) Zhu, K.; O'Keefe, C. A.; Vukotic, V. N.; Schurko, R. W.; Loeb, S. J. *Nat. Chem.* **2015**, *7*, 514−519.
(3) (a) Dominguez, Z.; Dang, H.; Strouse, M. J.; Garcia-Garibay, M. A. *J. Am. Chem. Soc.* **2002**, *124*, 2398−2399. (b) Comotti, A.; Bracco, S.; Yamamoto, A.; Beretta, M.; Hirukawa, T.; Tohnai, M.; Miyata, M.; Sozzani, P. *J. Am. Chem. Soc.* **2014**, *136*, 618−621.
(4) Kobr, L.; Zhao, K.; Shen, Y.; Comotti, A.; Bracco, S.; Shoemaker, R. K.; Sozzani, P.; Clark, N. A.; Price, J. C.; Rogers, C. T.; Michl, J. *J. Am. Chem. Soc.* **2012**, *134*, 10122−10131.
(5) (a) Gould, S. L.; Tranchemontagne, D.; Yaghi, O. M.; Garcia-Garibay, M. A. *J. Am. Chem. Soc.* **2008**, *130*, 3246−3247. (b) Winston, E. B.; Lowell, P. J.; Vacek, J.; Chocholoušová, J.; Michl, J.; Price, J. C. *Phys. Chem. Chem. Phys.* **2008**, *10*, 5188. (c) Kolokolov, D. I.; Stepanov, A. G.; Jobic, H. *J. Phys. Chem. C* **2014**, *118*, 15978−15984. Shustova, N. B.; McCarthy, B. D.; Dincă, M. *J. Am. Chem. Soc.* **2011**, *133*, 20126−20129.
(6) (a) Bracco, S.; Comotti, A.; Valsesia, P.; Chmelka, B. F.; Sozzani, P. *Chem. Commun.* **2008**, 4798−4800. (b) Bracco, S.; Beretta, M.; Cattaneo, A.; Comotti, A.; Falqui, A.; Zhao, K.; Rogers, C.; Sozzani, P. *Angew. Chem., Int. Ed.* **2015**, *54*, 4773−4777. (c) Vogelsberg, C. S.; Bracco, S.; Beretta, M.; Comotti, A.; Sozzani, P.; Garcia-Garibay, M. A. *J. Phys. Chem. B* **2012**, *116*, 1623−1632. (d) Comotti, A.; Bracco, S.; Valsesia, P.; Beretta, M.; Sozzani, P. *Angew. Chem., Int. Ed.* **2010**, *49*, 1760−1764.
(7) (a) O'Brien, Z. J.; Karlen, S. D.; Khan, S.; Garcia-Garibay, M. A. *J. Org. Chem.* **2010**, *75*, 2482−2491. (b) Comotti, A.; Bracco, S.; Ben, T.; Qiu, S.; Sozzani, P. *Angew. Chem., Int. Ed.* **2014**, *53*, 1043−1047.
(8) Desiraju, G. R. *Angew. Chem., Int. Ed. Engl.* **1995**, *34*, 2311−2327.
(9) Torres-Huerta, A.; Rodríguez-Molina, B.; Höpfl, H.; Garcia-Garibay, M. A. *Organometallics* **2014**, *33*, 354−362.
(10) (a) Corradi, E.; Meille, S. V.; Messina, M. T.; Metrangolo, P.; Resnati, G. *Angew. Chem., Int. Ed.* **2000**, *39*, 1782−1786. (b) Metrangolo, P.; Resnati, G. *Chem. - Eur. J.* **2001**, *7*, 2511−2519. (c) Metrangolo, P.; Meyer, F.; Pilati, T.; Resnati, G.; Terraneo, G. *Angew. Chem., Int. Ed.* **2008**, *47*, 6114−6127. (d) Priimagi, A.; Cavallo, G.; Metrangolo, P.; Resnati, G. *Acc. Chem. Res.* **2013**, *46*, 2686−2695.
(11) Lemouchi, C.; Vogelsberg, C. S.; Zorina, L.; Simonov, S.; Batail, P.; Brown, S.; Garcia-Garibay, M. *J. Am. Chem. Soc.* **2011**, *133*, 6371−6379.
(12) Le Questel, J.-Y.; Laurence, C.; Graton, J. *CrystEngComm* **2013**, *15*, 3212−3221.
(13) (a) Karlen, S. D.; Reyes, H.; Taylor, R. E.; Khan, S. I.; Hawthorne, M. F.; Garcia-Garibay, M. *Proc. Natl. Acad. Sci. U. S. A.* **2010**, *107*, 14973−14977. (b) Rodriguez-Molina, B.; Perez-Estrada, S.; Garcia-Garibay, M. A. *J. Am. Chem. Soc.* **2013**, *135*, 10388−10395.
(14) (a) Sauvajol, J. L. *J. Phys. C: Solid State Phys.* **1980**, *13*, L927−L934. (b) Zussman, A.; Alexander, S. *J. Chem. Phys.* **1968**, *48*, 3534−3539.
(15) (a) Cho, D. M.; Parkin, S. R.; Watson, M. D. *Org. Lett.* **2005**, *7*, 1067−1068. (b) Shishkin, O. V.; Shishkina, S. V.; Maleev, A. V.; Zubatyuk, R. I.; Vasylyeva, V.; Merz, K. *ChemPhysChem* **2013**, *14*, 847−856.
(16) Politzer, P.; Murray, J. S.; Clark, T. *Phys. Chem. Chem. Phys.* **2013**, *15*, 11178−11189.
(17) (a) Dunitz, J. D.; Schomaker, V.; Trueblood, K. N. *J. Phys. Chem.* **1988**, *92*, 856. (b) Dunitz, J.; Maverick, E. F.; Trueblood, K. N. *Angew. Chem., Int. Ed. Engl.* **1988**, *27*, 880−895.
(18) Fyfe, C. A. *Solid State NMR for Chemists*; CFC Press: Guelph, Ontario, 1983.
(19) Dinnocenzo, J. P.; Banach, T. E. *J. Am. Chem. Soc.* **1988**, *110*, 971−973.
(20) Nishikiori, S. I.; Soma, T.; Iwamoto, T. *J. Inclusion Phenom. Mol. Recognit. Chem.* **1997**, *27*, 233−243.

DOI: 10.1021/jacs.5b10776
J. Am. Chem. Soc. 2015, 137, 15386−15389